DOI: 10.1002/ejic.201000054

General Route to the Fabrication of ZnS and M-Doped (M = Cd^{2+}, Mn^{2+}, Co^{2+}, Ni^{2+}, and Eu^{3+}) ZnS Nanoclews and a Study of Their Properties

Lihong Dong,[a,b] Yang Liu,*[a] Yujiang Zhuo,[a] and Ying Chu*[a]

Keywords: Nanostructures / Doping / Heterogeneous catalysis / Zinc / Photochemistry

In a mixed solvent composed of water and ethylenediamine, pure and ion-doped (Cd^{2+}, Mn^{2+}, Co^{2+}, Ni^{2+}, Eu^{3+}, etc.) clew-like ZnS nanostructures, self-assembled by curled ZnS nanowires, were synthesized by means of a hydrothermal route. These nanoclews possess a high specific surface area and can be separated easily from solution by natural settlement due to the self-assembled structure; thus, they can be used in the field of photocatalysis. Photocatalytic experiments indicated that the pure ZnS nanoclews presented higher photocatalytic activity under UV irradiation, and the photocatalytic activity of the recycled ZnS nanoclews does not change noticeably after five reaction cycles. Furthermore, the $Cd_xZn_{1-x}S$ nanoclews showed high photocatalytic activity driven by visible light when the value of x was in the range from 0.3 to 0.7. The photoluminescence intensity of Eu^{3+}-doped ZnS nanoclews increased significantly compared with pure ZnS nanoclews. The formation mechanism of the ZnS nanoclews is also discussed.

Introduction

Recently, the large-scale self-assembly of meso-, micro-, and nanostructured building components has received much attention in the areas of materials synthesis and device fabrication.[1–5] Various one-, two-, and three-dimensional (1D, 2D, 3D) and curved architectures have been obtained,[6–10] thereby giving rise to the possibility of constituting a nanotoolbox for the "bottom-up" approach in nanoscience and nanotechnology.[11]

As an important wide-band-gap (3.6 eV) semiconductor, zinc sulfide (ZnS) has been used in diverse applications such as optical phosphors, catalysts, photonic crystals, and light-emitting materials.[12–15] In addition, ZnS has been examined as a photocatalyst, in part because of its high energy-conversion efficiency and the relatively negative redox potential of its conduction band.[16,17] For binary semiconductor ZnS nanostructures, band-gap energy is an important parameter in electronic and optoelectronic applications. The optical band gap of the semiconductor nanostructures can be tuned by changing their size. However, tuning the diameter and aspect ratio of 1D nanostructures is extremely challenging. Specifically, tuning the diameter of 1D nanostructures within the Bohr diameter range to achieve the desired band-gap tenability is critical. On the contrary, engineering the composition of the material is an alternative option to tuning the band gap of 1D nanostructures for specific applications.[18] It is well known that the addition of impurities into a wide-gap semiconductor can often induce dramatic changes in the optical, electrical, and magnetic properties.[19] Therefore, doping a selective element into ZnS nanostructures has become an important route for enhancing and controlling their optical, electrical, and magnetic performance, which is crucial for their practical applications, and recently many efforts have been focused on the preparation of doped ZnS nanostructures. For example, Ni^{2+}-doped ZnS hollow microspheres,[20] Cu^{2+}-doped ZnS nanorods[21] and hollow nanoparticles,[22] Mn^{2+}-doped ZnS nanocrystals[23] and nanorods,[24,25] and $Cd_{1-x}Zn_xS$ nanowires[18,26] have been synthesized by various methods, including ultrasonic spray pyrolysis, solvothermal processes, a hard template route, chemical vapor deposition processes, etc. Eu^{2+}-doped ZnS nanowires were also fabricated by the vapor deposition method.[27] Although the successes mentioned above have been obtained, as far as we aware, there has been no report on a general way to synthesize pure or multiple-ion-doped ZnS nanostructures, especially 3D nanostructures self-assembled by 1D nanowires. Furthermore, the creation of nanomaterials in solution is an art of arrested crystal growth that leads to materials that differ not only in size but also in shape.[28] Also, researchers have not stopped trying to employ environmentally friendly, simple, and low-cost methods in the fabrication of nanomaterials. Herein we report for the first time the mass fabrication of clew-like ZnS 3D microstructures (hereafter they will be called nanoclews for the sake of brevity) self-assembled by hexagonal wurtzite ZnS nanowires by means of a simple hydrothermal route in a mixed solvent of water and ethylenediamine. The photocatalytic degradation of methyl orange under UV irradiation revealed that these nanoclews

[a] Department of Chemistry, Northeast Normal University, Changchun 130024, P. R. China
Fax: +86-431-5684009
E-mail: chuying@nenu.edu.cn
liuy732@nenu.edu.cn
[b] Department of Chemistry, Tonghua Normal University, Tonghua 134002, P. R. China

had much higher photocatalytic activity than that of ZnS nanoparticles and P25-TiO_2 and could be separated easily, such as by natural settlement, because of their self-assembled structure. Furthermore, the photodecomposition activity decreased only slightly after five cycles of the photocatalytic experiments.

Because ZnS has an absorption edge at 329.2 nm, which limits its effectiveness to only the UV region of the solar spectrum (an efficient utilization of solar energy requires a response of the photocatalyst in the visible region), Cd^{2+} was incorporated into the ZnS nanoclews. With an increase in the doping amount of Cd^{2+}, the optical response of the $Cd_xZn_{1-x}S$ nanoclews gradually shifted into the visible region, and higher photocatalytic activity under visible-light irradiation was obtained. The synthesis method in this paper is also a general method that can potentially be extended to prepare other transition-metal-ion-doped (e.g., Mn^{2+}, Co^{2+}, Ni^{2+}) and rare-earth-ion-doped (e.g., Eu^{3+}) ZnS nanoclews, which makes the optical properties of ZnS nanoclews tunable and tailorable over a wide range. Moreover, a possible formation mechanism of the clew-like ZnS nanostructures is also proposed.

Results and Discussion

A typical panoramic SEM image of the ZnS nanoclews is presented in Figure 1a, in which the spherical clew-like morphology is clearly visible. The diameters of these self-assembly nanostructures are in the range of 2–5 μm. Figure 1b shows a magnified SEM image; closer inspection reveals that the as-obtained ZnS nanoclews are composed of large-scale curled nanowires with a diameter of 10–20 nm, and these nanowires twist around each other to form loose clew-like nanostructures. On account of the curled nature, it is hard to estimate the length of the nanowires. The XRD pattern of the product is given in Figure 1c, and all diffraction peaks can be conclusively indexed to hexagonal ZnS (JCPDS no. 75-1547). The strong and sharp diffraction peaks indicate that the as-obtained product is highly crystalline, and the slight peak broadening indicates that the nanowires have a small diameter. Compared with the standard pattern, the intensity of the [002] peak is unusually strong, thereby implying a possible preferential orientation growth along the [001] direction. No impurity phase can be detected. The energy-dispersive X-ray spectroscopy (EDS) result (Figure 1d) shows that the Zn/S atom ratio is 49:51 for the obtained product, which agrees well with the value calculated from the formula of ZnS.

Figure 2a shows a typical TEM image of the ZnS nanoclews, and a magnified TEM image (Figure 2b) further confirms that the diameter of the nanowires varies within 10–20 nm. It is also difficult to judge the length of the nanowires from the TEM images. The high-resolution (HR) TEM image of a single ZnS nanowire (Figure 2c) exhibits clear fringes perpendicular to the nanowire axis, the spacing of which measures 0.31 nm and agrees well with the interplanar spacing of the (002) planes of wurtzite ZnS. This

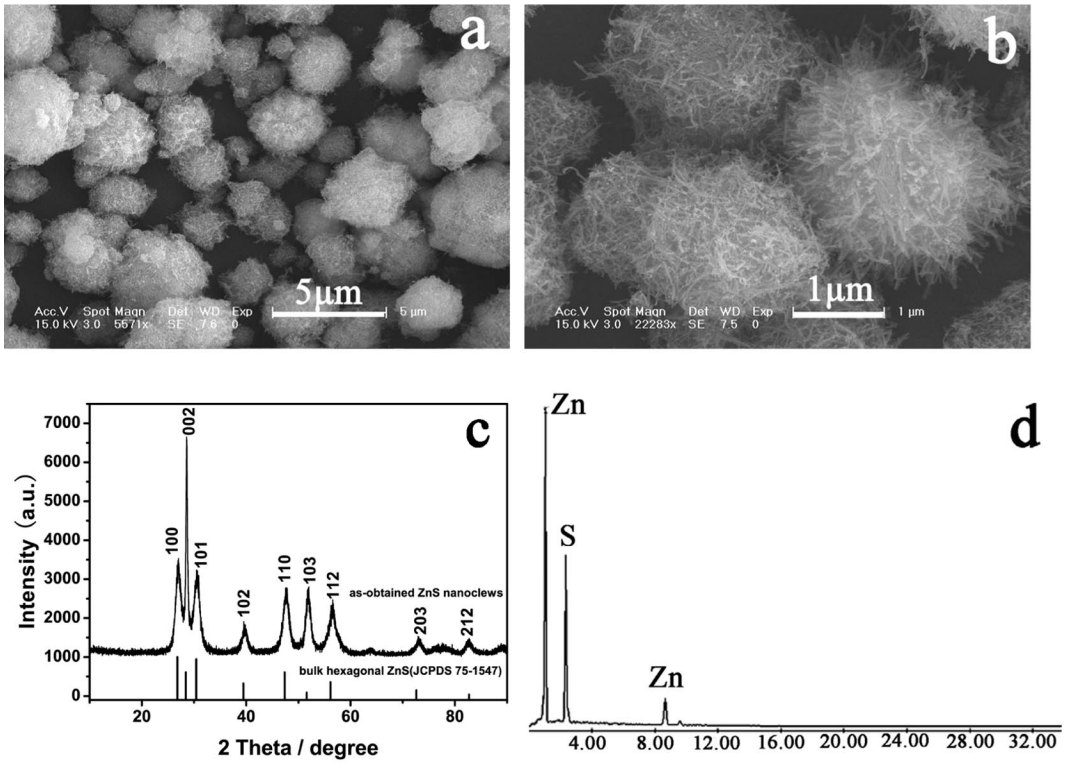

Figure 1. (a), (b) SEM images, (c) XRD pattern, and (d) EDS pattern of ZnS nanoclews. The vertical bars in (c) indicate the standard hexagonal ZnS peak position from JCPDS 75-1547.

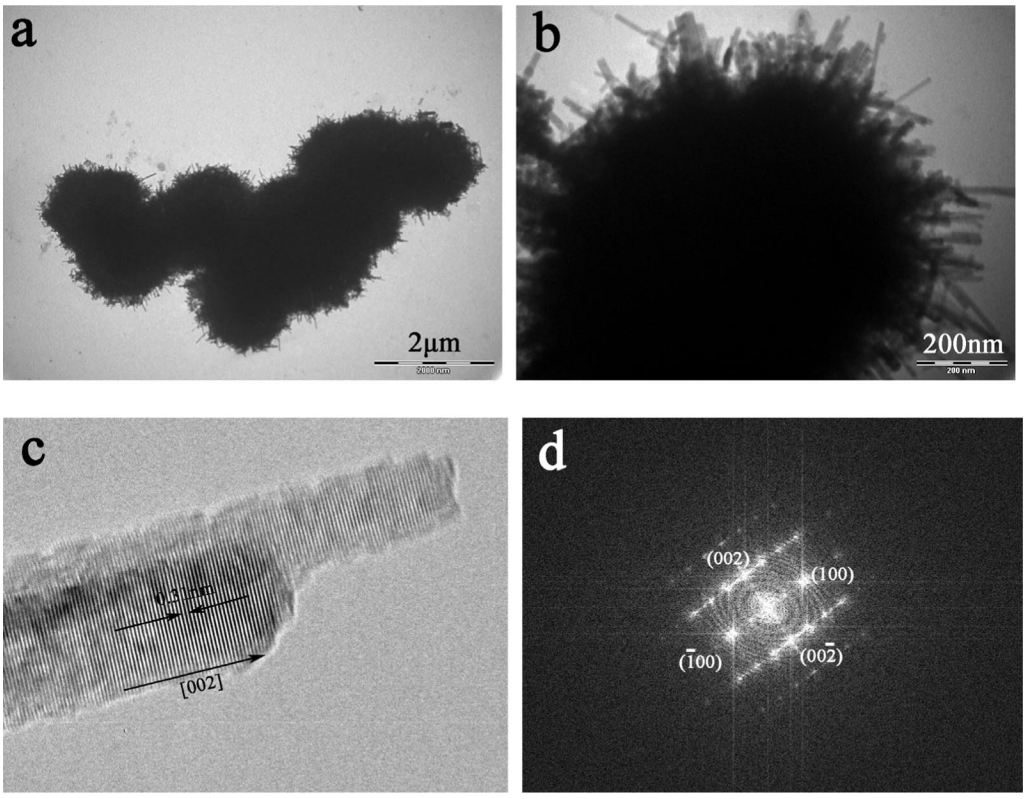

Figure 2. (a), (b) TEM images of ZnS nanoclews. (c) HRTEM image taken from a single nanowire. (d) FFT pattern obtained from a single nanowire.

is supported by the fast Fourier transform (FFT) pattern (Figure 2d). Clearly, the wurtzite ZnS nanowire grows along the [001] direction.

In Figure 3a, a nitrogen isotherm (adsorption–desorption loop) on the prepared ZnS nanoclews is displayed. The hysteresis loop typically belongs to type IV, thus indicating the characteristic of mesoporous materials. Our Brunauer–Emmett–Teller (BET) measurement indicates that the specific surface area of this sample is 135 $m^2 g^{-1}$, which is much higher than that of ZnS nanorods (51 $m^2 g^{-1}$).[31] Figure 3b shows the nitrogen isotherm of the prepared $Cd_{0.7}Zn_{0.3}S$ nanoclews, which also belongs to type IV; the BET specific surface area was measured to be 126 $m^2 g^{-1}$.

To shed light on the formation mechanism of the ZnS nanoclews, their growth process has been monitored by examining the products harvested at intervals of 0.5, 1, 3, 6, 12, and 24 h reaction time at 160 °C. The TEM image of the product harvested after a 0.5 h reaction is shown in Figure 4a. Nanostructures that look like downy velvet flowers made up of thin nanofilaments can be clearly observed. The length of the nanofilaments ranges from several hundred nanometers to 1 μm, and the diameter is about 10 nm. When the reaction time was prolonged to 1 h, relatively integrated nanoclews were the main product, as shown in Figure 4b. Through a continuous increase of the reaction time to 3 h, nanoclews became the exclusive product (the corre-

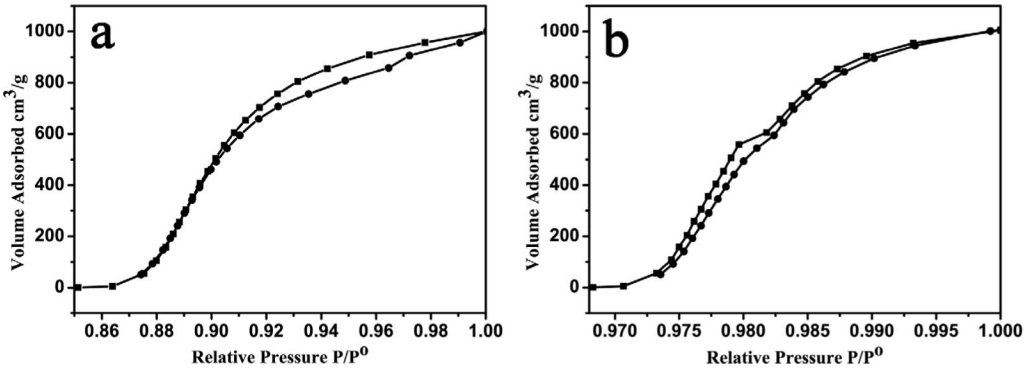

Figure 3. Adsorption–desorption isotherms of (a) ZnS nanoclews and (b) $Cd_{0.7}Zn_{0.3}S$ nanoclews.

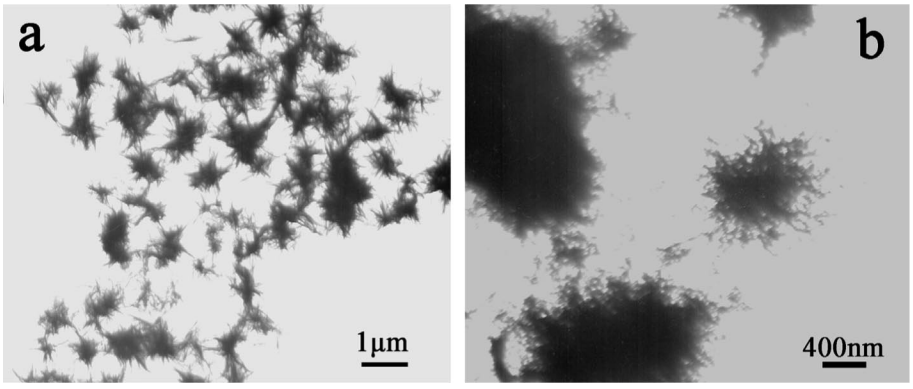

Figure 4. TEM images of the products harvested at different intervals: (a) 0.5 h and (b) 1 h.

sponding TEM image is similar to that in Figure 2a, so it is not shown here). But the nanowires were highly susceptible to melting during the TEM investigation, and a similar phenomenon can also be seen in Figure 4b, obtained by rapid operation, which is a possible result of the poor crystallinity of the nanowires. This problem could be solved by extending the reaction time; 12 h was sufficient to obtain ZnS nanoclews with better crystallinity, as mentioned in the previous paragraph.

As a kind of polydentate ligand, ethylenediamine has been widely used as solvent in the synthesis of one-dimensional nanostructures.[18,32–35] It was observed that, by mixing water with ethylenediamine in a 1:1 volume ratio, hexagonal ZnS nanorods were produced at 200 or 175 °C.[35] It is well known that hexagonal-phase ZnS is stable at temperatures higher than 1020 °C; the strong chelating ability of ethylenediamine together with high-pressure reaction conditions is believed to bring down the free-energy difference between the hexagonal and cubic phases of ZnS, thereby resulting in the formation of wurtzite ZnS at a lower temperature.[35] In wurtzite [space group *P*63*mc* (no. 186)], the S^{2-} anions form a hexagonal close-packed lattice along the crystallographic *c* direction with the Zn^{2+} cations occupying half of the tetrahedral holes. The unique structural feature of the (001) facet and the existence of a 63-screw axis along the *c* direction (the Donnay–Harker law)[36] lead to the anisotropic nature and significantly 1D-oriented preferable growth of hexagonal ZnS nanocrystals. Furthermore, ethylenediamine (en) molecules can adsorb on the surface (primarily on the six prismatic side planes) of ZnS by chelating the Zn^{2+} cations, which inhibits the radial enlargement of the wires and results in the formation of ZnS wires with a small diameter. On the basis of the above analyses and the experimental results, a growth mechanism of the ZnS nanoclews is proposed. At first, a relatively stable Zn–en complex formed. With the temperature elevated, thiourea (Tu) was attacked by the strong nucleophilic O atoms of H_2O molecules, thereby leading to the weakening of the C=S double bonds. The C=S bond would be broken, and the S^{2-} anion would be slowly generated, which would then react with Zn–en to form ZnS seeds. The decomposition temperature of Tu is above 150 °C (this was the reason we selected 160 °C as the synthesis temperature), so there were few S^{2-} anions being released in the initial stage. Upon increasing the temperature up to 160 °C, a great number of S^{2-} anions were released at this point, which caused an instantaneous explosive nucleation of ZnS. A great many of the initial nuclei also resulted in the formation of nanocrystals with a smaller size. Then, with the continuous supply of the building blocks, thin nanofilaments came into being (as shown in Figure 4a) because of the 1D-oriented preferable growth nature and the structure-directing effect of ethylenediamine. To minimize the Gibbs energy of the total system concomitant with the growth along the *c* axis to increase the aspect ratio, these nanofilaments self-assembled into bundles or flowers. It is well known that a sphere-like shape shows the lowest Gibbs energy relative to other shapes,[37] therefore, by prolonging the reaction time, sphere-like ZnS nanoclews that consisted of curled nanowires were obtained as the final product.

The concentration of $Zn(CH_3COO)_2$ played an important role in the formation of clew-like self-assembled nanostructures. It was found that when the reaction was carried out with half the typical concentration, namely 0.05 M, the product was composed of nanorods that coexisted with a few nanoclews. However, when the concentration of reactant was increased up to double the typical one, clew-like ZnS nanostructures were still the only product. The reason for the former should be that lower reactant concentrations led to less nucleation of ZnS and consequently fewer nanorods or nanowires; thus, the Gibbs energy of the system was not high enough to cause the self-assembly of nanoclews. Therefore, to obtain clewlike nanostructures, the concentration of the reactants must be above a certain value.

Temperature-dependent experiments also confirmed that it was correct to choose 160 °C as the synthesis temperature. Figure 5a shows a TEM image of the product obtained at 120 °C; it can be seen that many sheet-like nanostructures were the main product, which is the two-dimensional complex $ZnS{\cdot}(NH_2CH_2CH_2NH_2)_{0.5}$, as indicated by XRD results (Figure 5b).[38,39] A higher temperature, such as 200 °C, is not necessary because the products are still clew-like nanostructures.

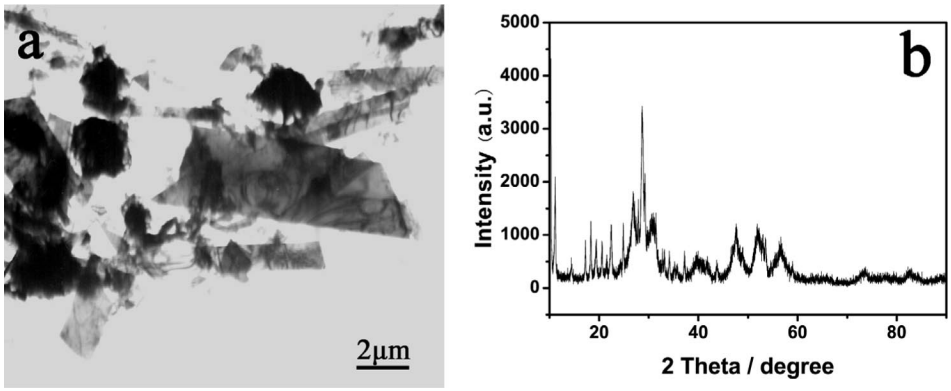

Figure 5. (a) TEM image and (b) XRD pattern of the product as-prepared at 120 °C.

As a result of their higher specific surface area and the ease with which they can be separated from solution by simple settlement, the ZnS nanoclews were used as solid-state catalysts and further investigated for their photocatalytic activity. Methyl orange (MO), a widely used dye, was selected as the model pollutant to evaluate the photocatalytic activity of the ZnS nanoclews. The characteristic absorption of 464 nm was chosen as the parameter monitored for the photocatalytic degradation process. Figure 6a shows the absorption spectra of an aqueous solution of MO in the presence of ZnS nanoclews measured after different times of exposure to the UV light. The absorption-peak intensity that corresponds to MO molecules decreases gradually as the exposure time increases, which indicates the photodegradation of MO. For the purpose of comparison, the photocatalytic degradation of MO without catalyst and with commercial TiO_2 powders (P25; Degussa), ZnS nanocrystals prepared according to a literature method,[29] and ZnS hollow nanospheres prepared according to our previous work[30] was carried out, and the results are illustrated in Figure 6c. In this figure, C_t is the absorption of MO at the wavelength of 464 nm, and C_0 is the absorption of MO after the adsorption equilibrium on photocatalysts before irradiation. Very little MO photodegradation can be observed without any catalyst under UV-light irradiation (less than 6.0% within 360 min), and it is also easily seen that the photocatalytic activity of the ZnS nanoclews is much higher than those of Degussa P25 TiO_2 and ZnS nanocrystals and is also much higher than that of ZnS hollow nanospheres. It took only 3 h to completely eliminate the MO by ZnS nanoclews. Whereas, after 3 h of the catalysis reaction, the degradation of MO was only 78% for ZnS hollow nanospheres, 85% for Degussa P25 TiO_2, and 61% for ZnS nanocrystals. The lower photocatalytic activity of the ZnS nanocrystals might result from the unwanted aggregation of ZnS nanocrystals during the photocatalytic process, which leads to a rapid decrease in the active surface area.[17] The photocatalytic superiority of ZnS nanoclews over ZnS hollow nanospheres may owe itself to the different crystal phases: the former is hexagonal ZnS and the latter is cubic ZnS. Moreover, the photocatalytic activity of the recycled ZnS nanoclews was also investigated, and the results are presented in Figure 6b. It can be seen that the photocatalytic activity of the recycled ZnS nanoclews does not change noticeably after five reaction cycles under UV irradiation, thereby indicating that the photocatalyst prepared in this study is stable and effective for the removal of MO in water. However, when the photodegradation of rhodium B (RhB) was performed with pure ZnS nanoclews under UV-light irradiation, as shown in Figure 6d, there still was about 30% residual RhB after 6 h of irradiation, and the efficiency was far lower than that for MO (Figure 6a). We attribute this phenomenon to the different adsorption ability on ZnS nanoclews between MO and RhB (i.e., MO was adsorbed more easily on the surface of ZnS nanoclews than RhB). However, the introduction of Cd ions into ZnS improved the adsorption level of RhB on the surface of ZnS nanoclews, which resulted in an increase of the photodegradation efficiency of RhB (the relative results will be discussed below in greater detail). Direct evidence for this hypothesis requires further study, and work is underway. From these results, it can also be concluded that the as-prepared ZnS nanoclews have a certain degree of selectivity in photocatalysis.

As mentioned in the Introduction, ZnS is a kind of wide-band-gap (3.77 eV) semiconductor with an absorption edge at 329.2 nm, which limits its effectiveness to only the UV region of the solar spectrum. An efficient utilization of solar energy requires the response of the photocatalyst in the visible region. An ideal way to address the above-mentioned challenge is to modulate its absorption into the visible-light range by doping, and CdS, as a kind of narrow-band-gap semiconductor (2.42 eV), came to mind. The reason for choosing the Cd ion is that it can be incorporated into the ZnS host throughout the doping region (i.e., x = 0–1), which has been proven by many experiments.[18,40] Moreover, the coordination ability of ethylenediamine to zinc is only slightly stronger than to cadmium {logβ of $[Zn(en)_3]^{2+}$ and $[Cd(en)_3]^{2+}$ are 14.11 and 12.18, respectively}. Therefore, it is expected that Cd-doped ZnS nanomaterials can be synthesized in the mixed solvent of ethylenediamine and water, and the band gap of $Cd_xZn_{1-x}S$ can be tuned by engineering the composition of the ternary semiconductor. Also, in comparison with pure CdS, $Cd_xZn_{1-x}S$ with its

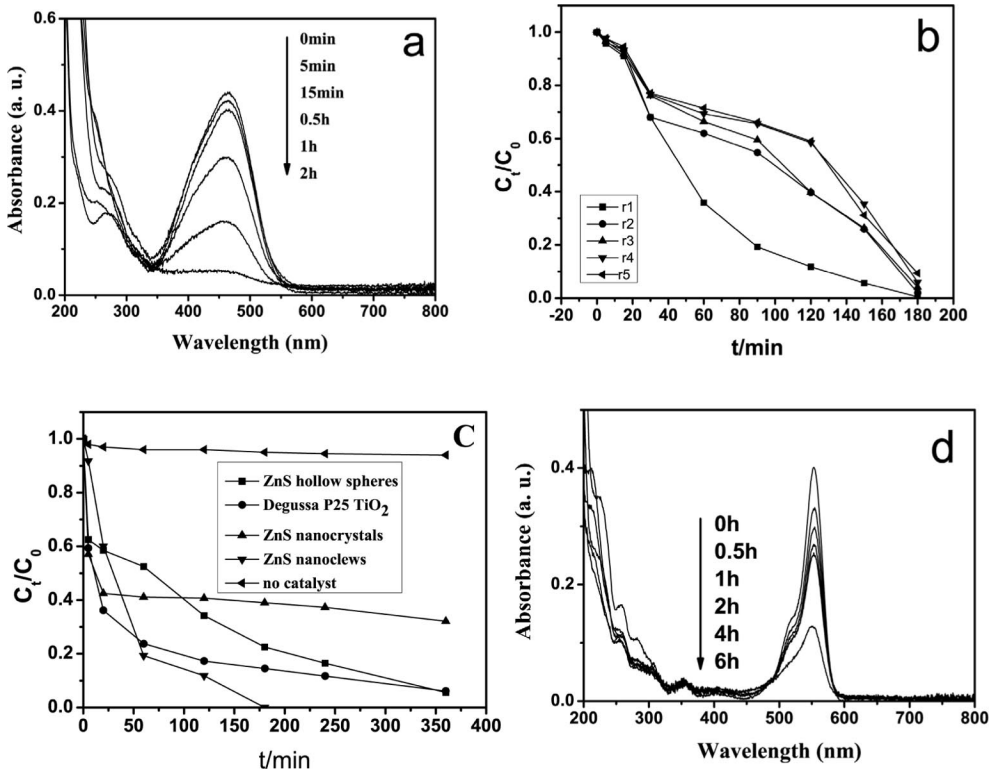

Figure 6. (a) Absorption spectra of an aqueous solution of MO in the presence of ZnS nanoclews measured after different times of exposure to UV light. (b) Degradation of methyl orange (MO) with recycled ZnS nanoclews. (c) Degradations of methyl orange without catalyst and with different photocatalysts under UV irradiation. (d) The absorption spectra of an aqueous solution of RhB in the presence of ZnS nanoclews measured after different times of exposure to the UV light.

wider band gap responds not only to visible light but also to UV light, which makes it a promising material for optoelectronic applications including photocatalysis.

Results of the TEM investigation indicated that the products obtained throughout the whole doping region (including the case of $x = 1$) all maintained the clew-like nanostructures composed of nanowires; a typical TEM image of product $Cd_{0.7}Zn_{0.3}S$ is shown in Figure 7a. Figure 7b gives the XRD patterns of the $Cd_xZn_{1-x}S$ samples with different compositions ($x = 0.0$, 0.05, 0.1, 0.3, 0.5, 0.7, and 0.9). It is obvious that all of the XRD peaks of the nanoclews can be indexed as the hexagonal wurtzite structure, which is consistent with the values on the standard JCPDS card. As the doping with Cd proceeds, the peak shifts slightly to a lower angle relative to that of the undoped ZnS nanoclews. Such a reduction in 2θ indicates that Cd atoms are gradually incorporated into the ZnS lattice, thus leading to the formation of the $Cd_xZn_{1-x}S$ nanowires. It also means the lattice constants of the products increase with an increase of the Cd content. The substitution of the Zn^{2+} ions ($r_{Zn^{2+}} = 0.74$ Å at tetrahedral sites) with the larger-radius Cd^{2+} ions ($r_{Cd^{2+}} = 0.92$ Å at tetrahedral sites) results in an increase in the lattice constants of ZnS.[40]

Figure 7c shows the UV/Vis absorption spectra of $Cd_xZn_{1-x}S$ with different x values. It can be seen that when $x = 0.7$, the absorption of the product in the visible range is the largest. So it can be speculated that the visible-light-driven photocatalytic ability of $Cd_{0.7}Zn_{0.3}S$ nanoclews may be the best. The BET surface area of the $Cd_{0.7}Zn_{0.3}S$ nanoclews is about 126 $m^2 g^{-1}$ (Figure 3b). This result implies that $Cd_{0.7}Zn_{0.3}S$ nanoclews may also have better photocatalytic ability over higher specific surface areas.

Figure 8 shows the temporal evolution of the spectral changes of MO mediated by $Cd_{0.7}Zn_{0.3}S$ nanoclews under visible-light irradiation. It can be seen that the concentration of MO decreases quickly, and the peak ($\lambda = 464$ nm) nearly disappears after 6 h, while a new peak ($\lambda = 245$ nm) emerges. Then the photoactivity of $Cd_{0.3}Zn_{0.7}S$ nanoclews was also investigated, and the result is shown in Figure 8b. Although the absorption of the product in the visible range is not as strong as that of $Cd_{0.7}Zn_{0.3}S$ nanoclews, the photoactivity of $Cd_{0.3}Zn_{0.7}S$ nanoclews driven by visible light is better than that of $Cd_{0.7}Zn_{0.3}S$ nanoclews. So it could be speculated that when the value of x is in the range of 0.3–0.7, the photocatalytic effect of $Cd_xZn_{1-x}S$ nanoclews is larger, and the photocatalysis experiment with $Cd_{0.5}Zn_{0.5}S$ nanoclews confirmed this speculation (Figure 8c). But further photocatalysis experiments indicated that the photoactivity of products with $x > 0.7$ and $x < 0.3$ (also including the case of $x = 1$) is less than that of the products with $0.3 < x < 0.7$ as indicated in Figure 8c. Figure 8c shows the photocatalytic performances of different $Cd_xZn_{1-x}S$ nanoclew photocatalysts determined by comparing the degradation efficiency of MO under otherwise identical conditions with visible-light illumination ($\lambda > 420$ nm). A blank test (MO without any catalyst) under visible light exhibited little

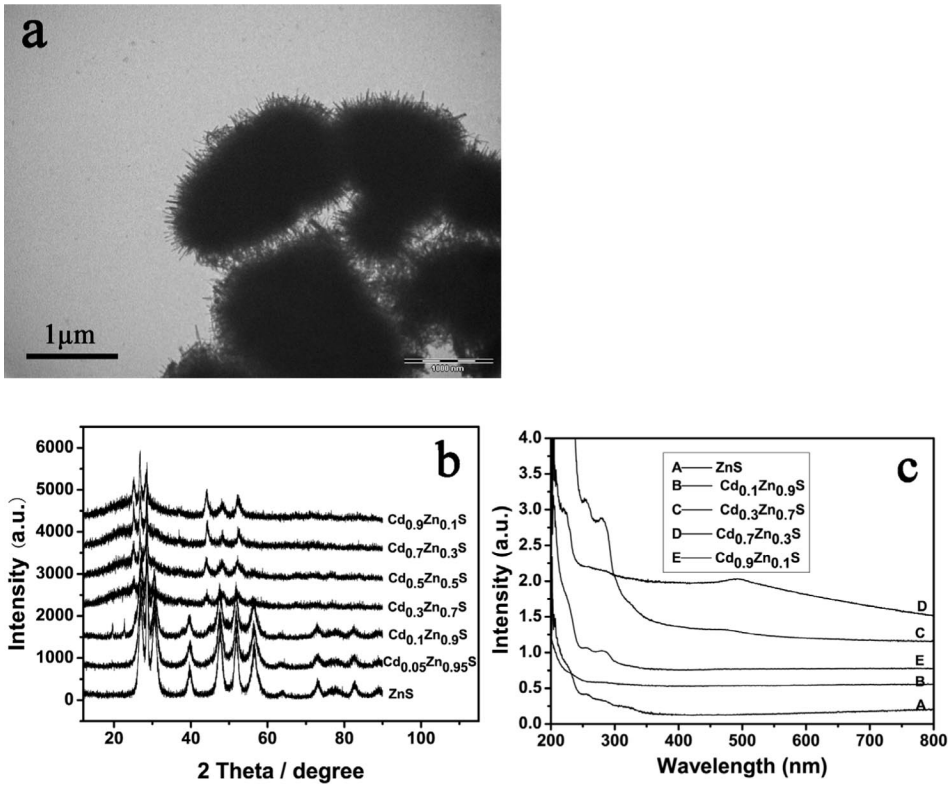

Figure 7. (a) TEM image of $Cd_{0.7}Zn_{0.3}S$ nanoclews. (b) X-ray diffraction pattern of $Cd_{1-x}Zn_xS$. (c) UV/Vis absorption spectra of $Cd_xZn_{1-x}S$.

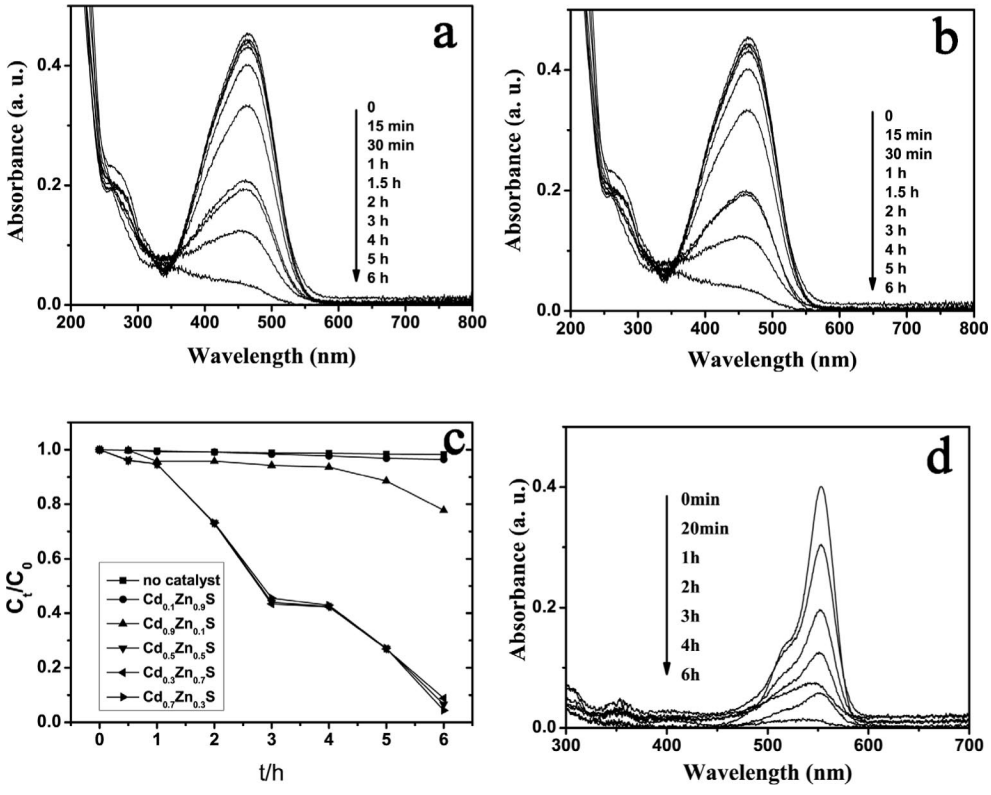

Figure 8. Temporal evolution of the spectra during the photodegradation of MO (or RhB) mediated by $Cd_xZn_{1-x}S$ nanoclews under visible-light illumination: (a) $Cd_{0.7}Zn_{0.3}S$/MO; (b) $Cd_{0.3}Zn_{0.7}S$/MO; (c) $Cd_xZn_{1-x}S$/MO; and (d) $Cd_{0.7}Zn_{0.3}S$/RhB.

photolysis, and the photodegradation efficiency was only 2% after 6 h, which demonstrated that the degradation of MO is extremely slow without a photocatalyst under visible-light illumination. The photodegradation efficiency of MO by $Cd_{0.1}Zn_{0.9}S$ just reached 4% after 6 h of reaction. Similarly, the photodegradation efficiency of MO by $Cd_{0.9}Zn_{0.1}S$ was only 22% after 6 h of visible-light irradiation. In the case of $0.3 < x < 0.7$, however, the photodegradation efficiency of MO reached nearly 100% after 6 h irradiation. On the basis of the experimental results, it could be proposed that a cooperative effect might exist between Zn and Cd in $Cd_xZn_{1-x}S$ nanoclews. When the ratio of Zn/Cd is close to 1, this kind of cooperative effect imbues $Cd_xZn_{1-x}S$ nanoclews with high photocatalytic activity. In contrast, when the ratio of Zn/Cd is far from 1, the cooperative effect is minimized, so the photodegradation efficiency is not high. Of course, the detailed mechanism that would account for the differences in photocatalytic activity that vary with the composition of $Cd_xZn_{1-x}S$ is still a puzzle in current research on nanomaterials, and more in-depth studies are necessary.

The photodegradation efficiency of RhB under visible-light irradiation was also carried out to investigate the universal applicability of the as-obtained $Cd_xZn_{1-x}S$ nanoclews, and the experimental results revealed that the $Cd_xZn_{1-x}S$ nanoclews also showed higher photocatalytic properties with RhB. The temporal UV/Vis spectral changes of an aqueous solution of RhB during the photocatalytic degradation reactions with $Cd_{0.7}Zn_{0.3}S$ nanoclews are depicted in Figure 8d. The main RhB absorbance markedly decreased with the prolongation of irradiation time and almost completely disappeared after 6 h of visible-light irradiation.

As ethylenediamine is a kind of didentate ligand it can coordinate with many ions. The method presented here should be suitable to prepare not only $Cd_xZn_{1-x}S$ but also other ion-doped ZnS nanostrucures. As expected, transition-metal-ion- (e.g., Mn^{2+}, Co^{2+}, Ni^{2+}) and rare-earth-ion-doped (e.g., Eu^{3+}) ZnS nanostrucures were obtained, and it is worth pointing out that the morphologies of the doped ZnS nanostrucures were all clew-like (Figure 9). Inductively coupled plasma (ICP) atomic emission spectroscopy measurements indicated that when the raw doping amount was 3% (relative to Zn), the actual doping amount was 2.99% for Mn, 2.45% for Co, 2.2% for Ni, and 2.89% for Eu, respectively.

Figures 9a and 10d show typical TEM and SEM images of Eu^{3+}-doped ZnS nanoclews (the doping amount is 3%). It can be seen that clew-like self-assembled nanostructures were preserved very well after the doping of Eu^{3+}. The corresponding XRD pattern is presented in Figure 10a, and the diffraction peaks can still be indexed to hexagonal wurtzite ZnS, thereby indicating that the crystal phase is also well maintained. On the other hand, further experiments indicated that impurities would appear when the amount of Eu^{3+} exceeded 5%, so the corresponding experimental results with amounts of Eu^{3+} larger than 5% are not discussed here. The EDS result of a raw doping amount

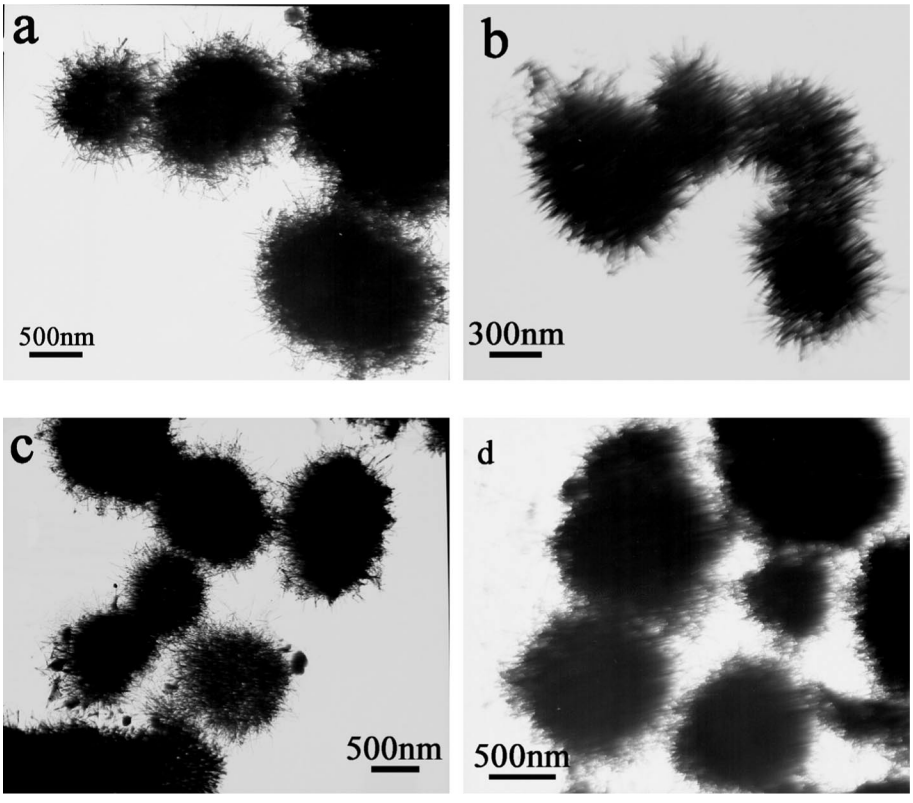

Figure 9. TEM images of ZnS nanoclews doped with different ions: (a) Eu^{3+}, (b) Mn^{2+}, (c) Co^{2+}, and (d) Ni^{2+}.

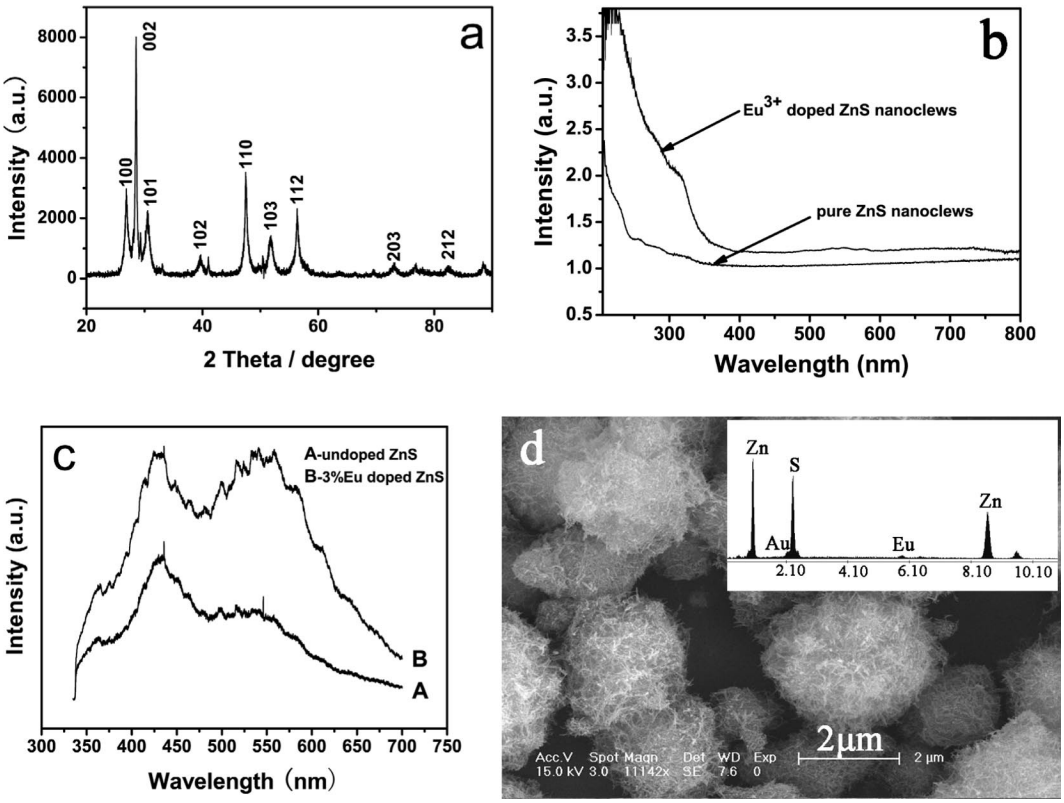

Figure 10. (a) XRD pattern, (b) UV/Vis spectra, and (c) PL spectra of the Eu^{3+}-doped ZnS nanoclews.

of 3% (inset in Figure 10d) shows that the atom ratio of Zn/Eu is 45.66:1.27, thereby indicating that the actual doping amount of Eu is 2.8% (relative to Zn), which is consistent with the ICP results and further confirms that Eu has been doped into the ZnS nanoclews. The UV/Vis spectra of the pure and Eu^{3+}-doped ZnS nanoclews are presented in Figure 10b. For pure ZnS nanoclews, an absorption peak at 319 nm is observed, which is close to the band-gap energy for the bulk hexagonal ZnS crystals (329 nm) and is believed to arise from the absorption of the near-band-edge free excitons. Compared with the pure ZnS nanoclews, the UV/Vis spectrum of Eu^{3+}-doped ZnS nanoclews has no obvious change for the absorption onset, thereby indicating that the size of the ZnS nanowires was not significantly influenced by the doping of Eu^{3+}; similar results have been reported.[27] The room-temperature photoluminescence (PL) spectra recorded from pure and Eu^{3+}-doped ZnS nanoclews are shown in Figure 10c. Compared with pure ZnS nanoclews, the intensity of Eu^{3+}-doped ZnS nanoclews increases significantly, especially the emission band at 548 nm.

Conclusion

A hydrothermal route in a mixed solvent composed of water and ethylenediamine was adopted for the general synthesis of pure and ion-doped (Cd^{2+}, Mn^{2+}, Co^{2+}, Ni^{2+} Eu^{3+}, etc.) clew-like ZnS nanostructures self-assembled by curled ZnS nanowires. Pure ZnS nanoclews presented higher photocatalytic activity under UV irradiation. Moreover, the photocatalytic activity of the recycled ZnS nanoclews does not change noticeably after five reaction cycles, thereby indicating a higher stability and effectiveness of the as-prepared product in photocatalytic applications. Moreover, the $Cd_xZn_{1-x}S$ nanoclews also showed high photocatalytic activity driven by visible light when the value of x is in the range of 0.3 to 0.7. After the doping with Eu^{3+}, the PL intensity of Eu^{3+}-doped ZnS nanoclews increased significantly compared with pure ZnS nanoclews, especially the emission band at 548 nm. By tuning and tailoring the component over a wide range, as-obtained pure and doped ZnS nanoclews could be widely used in optical, electronic, and magnetic fields.

Experimental Section

Material Preparation: All the reactants used were of analytical grade without any further purification before the experiment. For the synthesis of ZnS nanoclews, zinc acetate [$Zn(CH_3COO)_2{\cdot}2H_2O$; 2 mmol] and thiourea ($NH_2CSNH_2$, Tu; 6 mmol) were loaded into a Teflon-lined chamber with 50 mL capacity, which was filled to 80% of its total capacity with a mixture of ethylenediamine [$C_2H_4(NH_2)_2$, en] and deionized water in a 1:1 volume ratio. After being completely stirred, the autoclave was sealed and plaed into an oven that was maintained at 160 °C for 12 h and then cooled to room temperature naturally. The resulting white precipitates were collected and washed with deionized water several times. For the preparation of $Cd_xZn_{1-x}S$ and other ion-doped ZnS nanoclews, a desired amount of corresponding salts [$Cd(CH_3COO)_2{\cdot}2H_2O$,

$Mn(CH_3COO)_2{\cdot}4H_2O$, $CoCl_2{\cdot}6H_2O$, $Eu(NO_3)_3$] were introduced with the other conditions kept constant.

Photodegradation Reactions: In a typical experiment, as-obtained ZnS or $Cd_xZn_{1-x}S$ nanoclew catalyst (20 mg) was added to deionized water (34 mL) in a 100 mL conical flask. The mixture was subjected to ultrasonic treatment in a water bath for 15 min to ensure a good dispersion of the catalysts, followed by the addition of methyl orange solution ($C_{14}H_{14}N_3NaO_3S$, MO; 200 mg L^{-1}, 16 mL). The flask was sealed and the mixture stirred at room temperature for 15 min to achieve adsorption equilibrium for methyl orange. The mixture was later illuminated with an Hg lamp (100 W) or Xe lamp (300 W), during which a samples (3.0 mL) of the solution together with the catalyst were drawn at given time intervals to determine the concentration of the remaining reactant by using UV/Vis spectrophotometry; the solution was separated from the catalyst by settlement for about 15 min. For comparison purposes, commercial TiO_2 powders (P25; from Degussa), ZnS nanocrystals prepared according to a literature method,[29] and ZnS hollow nanospheres prepared according to our previous work[30] were also tested as references. The chemical stability of the ZnS nanoclew catalyst was further tested after five cycles of the reaction. In this test, the used catalyst after separation was mixed immediately with a newly prepared methyl orange solution [34 mL of deionized water and 16 mL of the methyl orange solution (200 mg L^{-1})]. Then the photocatalysis reaction was repeated under the same conditions.

Material Characterization: The phase purities of all the obtained samples were measured with a Rigaku X-ray diffractometer with Cu-K_α radiation (λ = 1.5406 Å). A small amount of the product was dispersed in ethanol by ultrasonic treatment for approximately 10 min. Then one drop of the resulting solution was placed onto a carbon-coated copper grid and dried at room temperature for the next TEM and HRTEM visualization. The lower-resolution TEM images were recorded with a Hitachi H-800 transmission electron microscope, and HRTEM lattice images and selected-area electron diffraction (SAED) results were obtained with a JEOL JEM-2010 high-resolution transmission electron microscope operating at 200 kV. Field-emission scanning electron microscopy (FESEM), together with EDS were conducted with a field-emission scanning electron microscope (JEOL, 7500B). Nitrogen adsorption measurements were performed with a Hiden Isochema Intelligent Gravimetric Analyzer (IGA-100) system. The photoluminescence (PL) emission spectra were measured by using an excitation wavelength of 325 nm with a power of 50 mW, and performed with a LABRAM-UV Raman microspectrometer (Jobin Yvon).

Acknowledgments

This work was supported by the Natural Science Fund of China (nos. 20573017 and 20803008) and the Analysis and Testing Foundation of Northeast Normal University.

[1] Y. Huang, X. F. Duan, Q. Q. Wei, C. M. Lieber, *Science* **2001**, *291*, 630–633.
[2] G. M. Whitesides, B. Grzybowski, *Science* **2002**, *295*, 2418–2421.
[3] V. R. Thalladi, G. M. Whitesides, *J. Am. Chem. Soc.* **2002**, *124*, 3520–3521.
[4] H. Cölfen, S. Mann, *Angew. Chem. Int. Ed.* **2003**, *42*, 2350–2365.
[5] P. Yang, *Nature* **2003**, *425*, 243–244.
[6] D. H. Gracias, J. Tien, T. L. Breen, C. Hsu, G. M. Whitesides, *Science* **2000**, *289*, 1170–1172.
[7] H. Shi, L. Qi, J. Ma, H. Cheng, *J. Am. Chem. Soc.* **2003**, *125*, 3450–3451.
[8] H. Wu, V. R. Thalladi, S. Whitesides, G. M. Whitesides, *J. Am. Chem. Soc.* **2002**, *124*, 14495–14502.
[9] P. A. Smith, C. D. Nordquist, T. N. Jackson, T. S. Mayer, R. Martin, J. Mbindyo, T. E. Mallouk, *Appl. Phys. Lett.* **2000**, *77*, 1399–1401.
[10] S. Liu, H. W. Zhang, M. T. Swihart, *Nanotechnology* **2009**, *20*, 235603.
[11] G. R. Patzke, F. Krumeich, R. Nesper, *Angew. Chem. Int. Ed.* **2002**, *41*, 2446–2461.
[12] A. Wolosiuk, O. Armagan, P. V. Braun, *J. Am. Chem. Soc.* **2005**, *127*, 16356–16357.
[13] B. Xia, I. W. Lenggoro, K. Okuyama, *Chem. Mater.* **2002**, *14*, 4969–4974.
[14] I. D. Hosein, C. M. Liddell, *Langmuir* **2007**, *23*, 2892–2897.
[15] Z. Quan, Z. Wang, P. Yang, J. Lin, J. Fang, *Inorg. Chem.* **2007**, *46*, 1354–1360.
[16] J. S. Hu, L. L. Ren, Y. G. Guo, H. P. Liang, A. M. Cao, L. J. Wan, C. L. Bai, *Angew. Chem. Int. Ed.* **2005**, *44*, 1269–1273.
[17] Q. Zhao, Y. Xie, Z. Zhang, X. Bai, *Cryst. Growth Des.* **2007**, *7*, 153–158.
[18] S. Biswas, S. Kar, S. Santra, Y. Jompol, M. Arif, S. I. Khondaker, *J. Phys. Chem. C* **2009**, *113*, 3617–3624.
[19] G. Sanon, R. Rup, A. Mansingh, *Phys. Rev. B* **1991**, *44*, 5672–5680.
[20] J. H. Bang, R. J. Helmich, K. S. Suslick, *Adv. Mater.* **2008**, *20*, 2599–2603.
[21] A. Datta, S. K. Panda, S. Chaudhuri, *J. Solid State Chem.* **2008**, *181*, 2332–2337.
[22] T. Arai, S. Senda, Y. Sato, H. Takahashi, K. Shinoda, B. Jeyadevan, K. Tohji, *Chem. Mater.* **2008**, *20*, 1997–2000.
[23] X. F. Wang, J. J. Xu, H. Y. Chen, *J. Phys. Chem. C* **2008**, *112*, 17581–17585.
[24] S. Kar, S. Biswas, *J. Phys. Chem. C* **2008**, *112*, 11144–11149.
[25] S. Delikanli, S. He, Y. Qin, P. Zhang, H. Zeng, H. Zhang, M. Swihart, *Appl. Phys. Lett.* **2008**, *93*, 132501.
[26] Y. F. Lin, Y. J. Hsu, S. Y. Lu, K. T. Chen, T. Y. Tseng, *J. Phys. Chem. C* **2007**, *111*, 13418–13426.
[27] B. C. Chen, Z. G. Wang, *Adv. Funct. Mater.* **2005**, *15*, 1883–1890.
[28] U. K. Gautam, L. S. Panchakarla, B. Dierre, X. Fang, Y. Bando, T. Sekiguchi, A. Govindaraj, D. Golberg, C. N. Rao, *Adv. Funct. Mater.* **2009**, *19*, 131–140.
[29] C. L. Torres-Martínez, R. Kho, O. I. Mian, R. K. Mehra, *J. Colloid Interface Sci.* **2001**, *240*, 525–532.
[30] L. H. Dong, Y. Chu, Y. P. Zhang, Y. Liu, F. Y. Yang, *J. Colloid Interface Sci.* **2007**, *308*, 258–264.
[31] G. C. Xi, C. Wang, X. Wang, Q. Zhang, H. Q. Xiao, *J. Phys. Chem. C* **2008**, *112*, 1946–1952.
[32] J. Yang, J. H. Zeng, S. H. Yu, L. Yang, G. E. Zhou, Y. T. Qian, *Chem. Mater.* **2000**, *12*, 3259–3263.
[33] B. Liu, H. C. Zeng, *J. Am. Chem. Soc.* **2003**, *125*, 4430–4431.
[34] P. T. Zhao, K. X. Huang, *Cryst. Growth Des.* **2008**, *8*, 717–722.
[35] S. Biswas, S. Kar, S. Chaudhuri, *J. Phys. Chem. B* **2005**, *109*, 17526–17530.
[36] X. G. Peng, L. Manna, W. D. Yang, J. Wickham, E. Scher, A. Kadavanich, A. P. Alivisatos, *Nature* **2000**, *404*, 59–61.
[37] Z. A. Peng, X. G. Peng, *J. Am. Chem. Soc.* **2002**, *124*, 3343–3353.
[38] S. H. Yu, M. Yoshimura, *Adv. Mater.* **2002**, *14*, 296–300.
[39] Z. X. Deng, C. Wang, X. M. Sun, Y. D. Li, *Inorg. Chem.* **2002**, *41*, 869–873.
[40] D. S. Kim, Y. J. Cho, J. Park, *J. Phys. Chem. C* **2007**, *111*, 10861–10868.

Received: January 21, 2010
Published Online: May 4, 2010

